Orientation-dependent forward-backward photoelectron holography from asymmetric molecules

Xue-Bin Bian[1,2,*] and André D. Bandrauk[2]

[1]*State Key Laboratory of Magnetic Resonance and Atomic and Molecular Physics, Wuhan Institute of Physics and Mathematics, Chinese Academy of Sciences, Wuhan 430071, People's Republic of China*

[2]*Laboratoire de chimie théorique, Département de Chimie, Université de Sherbrooke, Sherbrooke, Quebéc, Canada J1K 2R1*

(Received 4 October 2013; published 24 March 2014)

Orientation-dependent photoelectron holography from the one-electron polar molecular ion HeH^{2+} in linearly polarized few-cycle laser fields is studied numerically. We identify four dominant holography patterns simultaneously with one shot of lasers and show that these are sensitive to the molecular structure and the orientation angle between the molecular axis and laser polarization direction. Due to the preferential enhanced ionization from one direction of the molecular axis, two kinds of forward photoelectron holography and two backward holography interference patterns predicted by a semiclassical model show up simultaneously for parallel orientation. Coulomb focusing effects are shown to be crucial for the backward scattering holography and a weak forward scattering holography channel with relatively small overlap. In contrast, after increasing the orientation angle, the backward scattering patterns disappears gradually because of the smaller scattering cross sections. Only one forward scattering holography can be clearly identified in the perpendicular orientation. Ultrashort and intense laser pulses are shown to be preferred for photoelectron holography. Intercycle interference rings in the above-threshold ionization are suppressed and consequently the intracycle rescattering signals are enhanced.

DOI: 10.1103/PhysRevA.89.033423 PACS number(s): 32.80.Wr, 33.60.+q, 61.05.jp

Holography first proposed by Gabor [1] is widely used in optical physics. The central idea of holography is to use a *reference* wave to interfere with a *signal* wave and record the relative phase and amplitude. The signals can be retrieved after knowing the holography pattern and *reference* waves. With the development of intense ultrashort laser pulses, photoelectron imaging and holography [2–7] has recently attracted a lot of attention in the study of strong laser-matter interactions. In the above-threshold ionization (ATI) of atoms and molecules in strong laser fields, laser-induced holography occurs naturally. Part of photoelectrons can be driven back after ionization to be rescattered by the atomic and molecular cores [8–10]. Another part of the photoelectrons are driven by the laser field to detectors directly. The former act as *signal* waves, which encode the structure of the cores after rescattering. The latter can be viewed as *reference* waves. After measuring the final momentum of the *reference* electrons, their phase and birth (ionization) times can be determined by a semiclassical model [7–10]. As a result, the photoelectron holography imprints rich information of the ultrafast scattering process and can be decoded by the semiclassical model such as the strong-field approximation (SFA) used in imaging [3].

Photoelectron holography was experimentally observed by Huismans *et al.* [4] using a long-wavelength 7 μm free-electron laser (FEL). This low-frequency laser favors the forward scattering of the photoelectrons due to the wide spread of electron wave packets. It has been shown that there are four kinds of photoelectron holography patterns predicted by the semiclassical model [7] based on recollision physics [3,9,10]. These patterns include two forward scattering patterns and two backward scattering patterns. They are of subcycle interference dynamics. However, the second kind of forward scattering patterns has not been identified in the ATI of Xe [4]. It has not been confirmed even in quantum simulations. The overlap between the *signal* and *reference* trajectories is relatively small with long-wavelength lasers. It may also be hidden by ATI rings in long laser pulses and it has not been resolved. Long-wavelength lasers are not a necessary condition to resolve photoelectron holography [11]. To observe the backward scattering holography, molecular ions with multiple centers and short-wavelength laser fields can be used as shown in Ref. [6]. The Coulomb focusing effect [12], which can increase the scattering cross sections, is shown to be crucial in observing backward scattering holography. The energy of the scattered photoelectrons can be controlled up to 10 U_p ($U_p = I/4\omega^2$ denotes the ponderomotive energy.). Their corresponding de Broglie wavelength $\lambda_e = 2\pi/p$ can be made comparable to or even smaller than molecular distances R by varying the frequency ω and intensity I of the incident pulses. Photoelectron holography [6] can thus provide attosecond (1 as $= 10^{-18}$ s) time-resolved tools for dynamic imaging of molecular structure [13–16].

Due to permanent dipoles, polar molecules have received increasing attention recently [17–22]. In this article we study the orientation [23,24] dependence of photoelectron holography in linearly polarized laser fields for the one-electron polar molecular ion HeH^{2+}. The phenomena of enhanced excitation (EE) and enhanced ionization (EI) have been reported [17] as essential phenomena in polar molecules. The electron in the ground state is preexcited to a localized resonant excited state with a long lifetime [25] first, then it is ionized and oscillates in the laser field acquiring kinetic energy. Resonant EE plays a very important role in EI. However, EE is sensitive to the orientation effect, and has a strong influence in the photoelectron holography as shown here.

We investigate photoelectron holography from the one-electron HeH^{2+} using accurate numerical methods. To provide an insight into the physical process behind photoelectron holography, a classical model based on Newton equations of motion is solved. It has been shown that the multiple rescattering of photoelectrons by laser pulses can be identified

*xuebin.bian@wipm.ac.cn

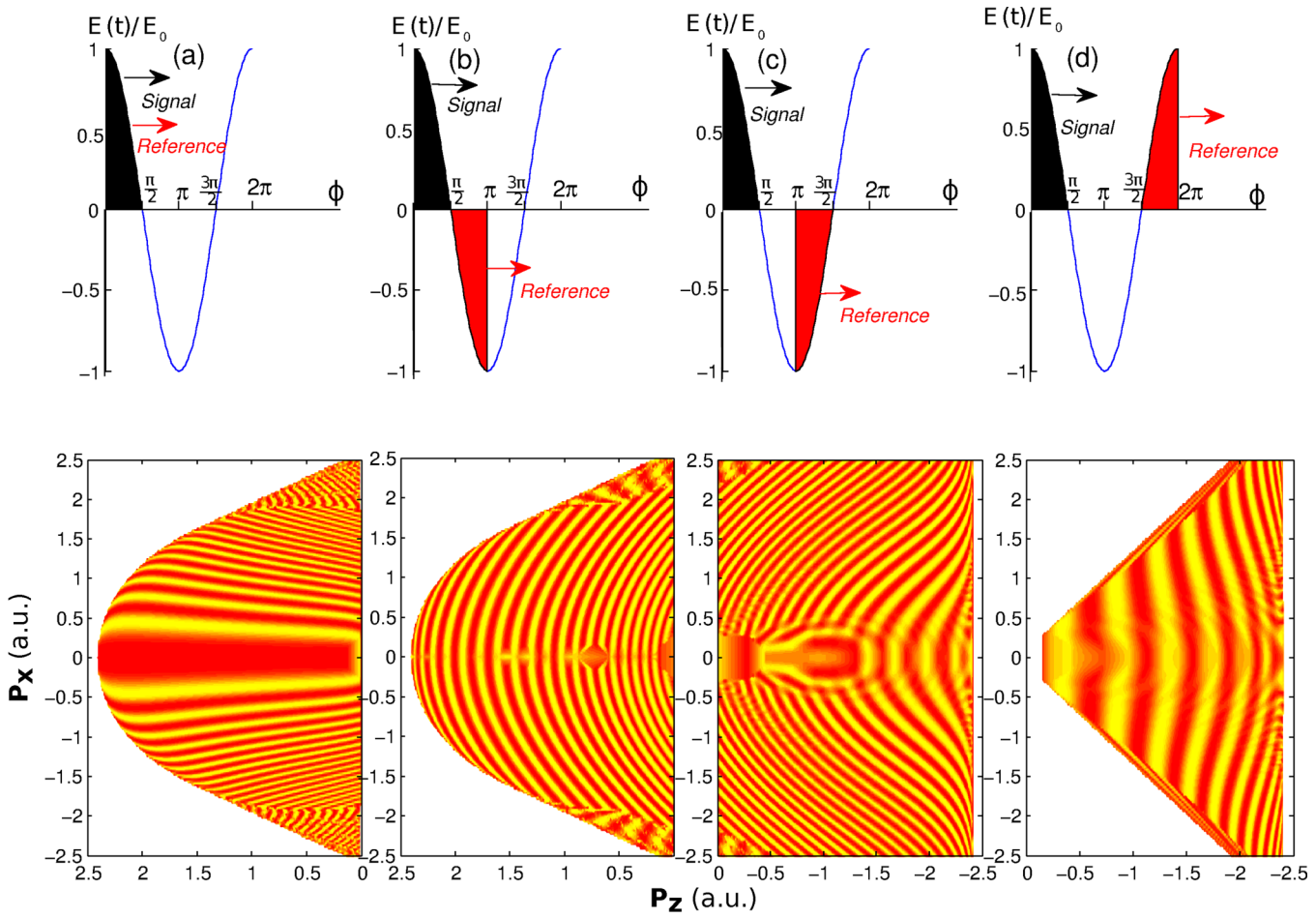

FIG. 1. (Color online) Photoelectron holography patterns predicted by a semiclassical model. In the upper panel, the signal electrons are set to be ionized in the first quarter cycle. The reference electrons may be ionized from the same quarter or other three quarter cycles. In the lower panel, (a) and (b) are forward scattering interference patterns, while (c) and (d) correspond to backward scattering interference patterns. The laser intensity is $I = 1.6 \times 10^{15}$ W/cm^2, and the wavelength is $\lambda = 532$ nm. The polarization of the field is along the z axis. The ionization potential corresponds the ground state of HeH^{2+} with internuclear distance $R = 4$ a.u. Stark shift of energy levels are included in the calculations.

in the low-energy features of the momentum spectra [26–28]. Although clear low-energy structure can be resolved in our quantum simulations, we emphasize one-recollision events in the ultrafast process in the present work. The ionization time of *signal* electrons is fixed in the first quarter cycle of the laser pulse, while the *reference* electrons ionization may occur in the same or different quarter cycles. The ground-state electrons are concentrated on the He^{2+} ion [24] due to the higher nuclear charge as compared to H^+, so we neglect the scattering by H^+ in this model. Due to the permanent dipole of the asymmetric molecule, the Stark shift of the energy level cannot be ignored. The ionization potential is approximately written as $I_p(t) = I_p(0) - 3RE(t)/5$ for parallel orientation [17] during our calculations for the phase difference between the *signal* and *reference* channels. For more details of the calculations, we refer readers to Refs. [6,7]. The laser polarization is along the z axis. The laser intensity is $I = 1.6 \times 10^{15}$ W/cm^2, the wavelength is $\lambda = 532$ nm. The internuclear distance of HeH^{2+} is fixed at $R = 4$ a.u., close to the excited-state minimum $R = 3.89$ a.u. The ionization potential of the ground state is $I_p = 2.25$ a.u. The obtained holography patterns are illustrated in Fig. 1. In Figs. 1(a) and 1(b) the interference patterns correspond to forward scattering of photoelectrons. The last two are backward scattering interference patterns. One can see that the four kinds of holography patterns are quite different. In Fig. 1(a) the pattern is spread and distributed angularly. In Fig. 1 (b) the patterns occur as radial semirings. It is to be noted that they are quite different from ATI rings. The radius of ATI rings in momentum space is proportional to $\sqrt{2n\omega}$ (a.u.). The density of the rings becomes high as the value of n increases. However, in Fig. 1(b), the space between the rings increases as $|P_z|$ increases. The width of the rings also increases as the value of n becomes high. Figure 1(c) represents incoming semirings as opposed to outgoing rings in Fig. 1(b). The main distribution of the structure occurs at smaller $|P_x|$, similar to Fig. 1(a). The density of stripes in Fig. 1(d) becomes higher as $|P_z|$ increases, as opposed to Figs. 1(b) and 1(c), where the density decreases. The subcycle interference dynamics makes the holography patterns clearly visible for a wide range of laser parameters, such as wavelength, intensity, and durations [7,29]. It guarantees the identification of the patterns in ATI.

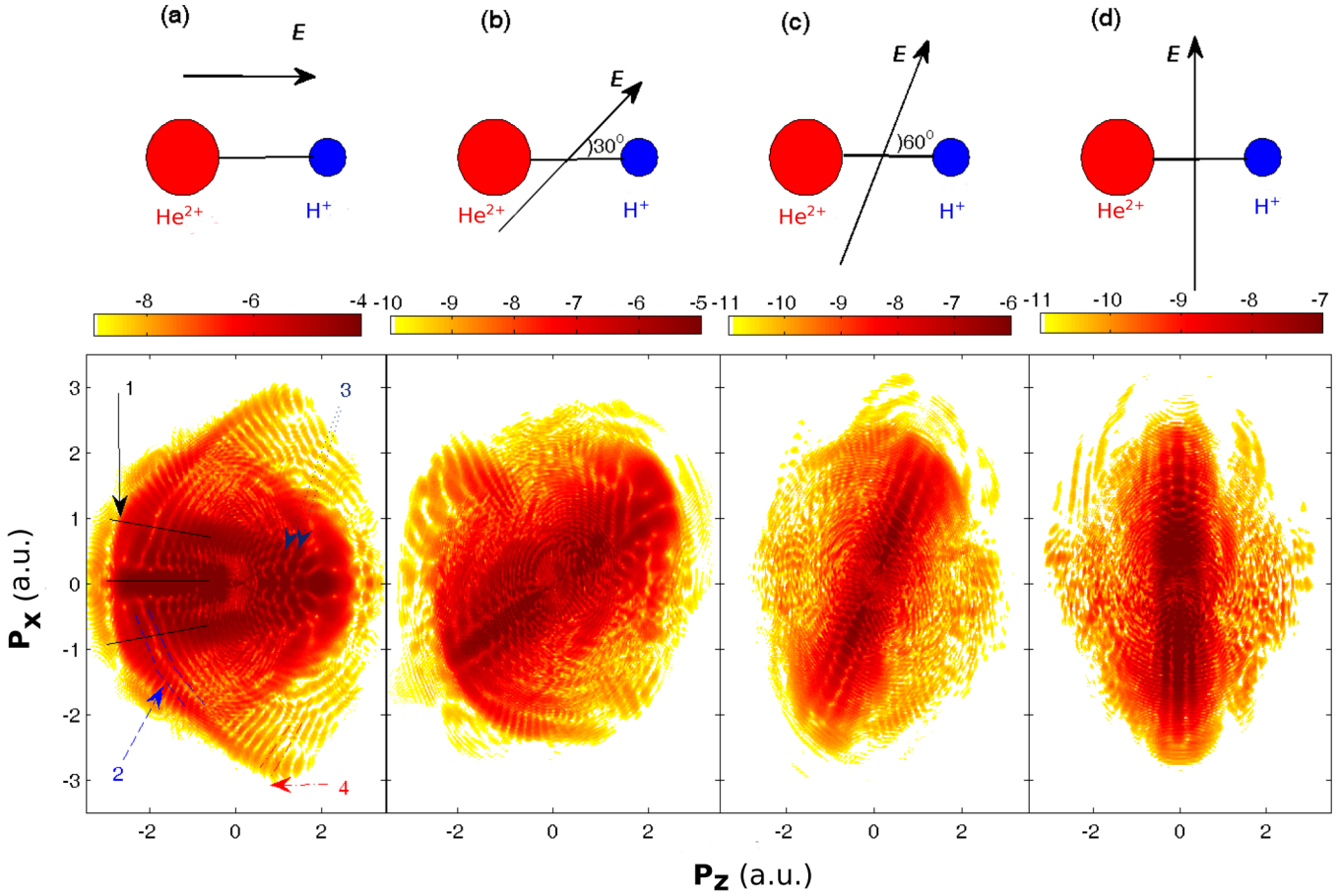

FIG. 2. (Color online) Molecular geometry of HeH^{2+} in linearly polarized laser fields (upper panel) and the corresponding photoelectron momentum distribution calculated by solving TDSE (lower panel, the color is plotted on the logarithmic scale.). The laser parameters are the same as in Fig. 1. The total pulse duration is five optical cycles. In the lower panel of (a), the marked 1, 2, 3, and 4 correspond to the four interference channels as illustrated in Fig. 1.

We also simulate the photoelectron momentum distribution of HeH^{2+} for the above laser field by solving the full-dimensional time-dependent Schrödinger equations (TDSE). Spherical coordinates are adopted in our calculations. The field-free Hamiltonian in the Born-Oppenheimer approximation (BOA) is (atomic units are used throughout, $e = \hbar = m_e = 1$)

$$H_0 = -\frac{1}{2}\nabla^2 - \frac{Z_2}{|\mathbf{r}+\mathbf{R}/2|} - \frac{Z_1}{|\mathbf{r}-\mathbf{R}/2|}, \tag{1}$$

where R is the nuclear distance, and Z_1 and Z_2 are nuclear charges, respectively. A multipole expansion of the nuclear attraction potential gives [24]

$$\frac{1}{|\mathbf{r}-\mathbf{R}/2|} = \sum_{\lambda=0}^{\infty} \frac{r_<^\lambda}{r_>^{\lambda+1}} P_\lambda(\cos\theta). \tag{2}$$

Here $r_<(r_>)$ is the smaller (larger) one of the r and $R/2$, and $P_\lambda(\cos\theta)$ are the Legendre polynomials.

The wave function is expanded by B splines [24]:

$$\Psi(r,\xi,\phi) = \sum_{i,j,m} C_{i,j}^m B_i(r)(1-\xi^2)^{\frac{|m|}{2}} B_j(\xi)\frac{\exp(im\phi)}{\sqrt{2\pi}}, \tag{3}$$

with $\xi = \cos\theta$.

The corresponding TDSE is written as

$$i\frac{\partial}{\partial t}\Psi(\mathbf{r},t) = [H_0 + H(t)]\Psi(\mathbf{r},t), \tag{4}$$

where the interaction term in velocity gauge is defined as $H(t) = \mathbf{A}(t)\cdot\mathbf{P}$. We set the molecular axis along the z axis, which has an angle χ with the laser polarization direction in the xz plane as illustrated in Fig. 2. The vector potential of the laser pulse is given by $\mathbf{A}(t) = E_0/\omega f(t)\cos(\omega t)\hat{\mathbf{e}}$, $t \in [-\tau/2,\tau/2]$, with the pulse shape $f(t) = \cos^2(\pi t/\tau)$, τ is the total duration of the laser pulses. Thus $A(\pm\tau/2) = 0$, ensuring the zero area condition $\int_{-\tau/2}^{\tau/2} E(t)dt = 0$. The total duration in our calculations is $\tau = 5$ cycles, which corresponds to the FWHM of the pulse around 4.5 fs (1 fs $= 10^{-15}$ s). It is short compared to molecular vibrational periods. We have also checked our calculations in a range of internuclear distance $R = 3$–6 a.u. The patterns presented in this work are little changed. Our calculations based on BOA is reasonable. The time propagation scheme used is the Crank-Nicolson method, which expresses the exponential operator to the third order as

$$\exp(-iH\Delta t) = \frac{1 - iH\Delta t/2}{1 + iH\Delta t/2} + O(\Delta t^3). \tag{5}$$

We have built an efficient parallel code to solve the above full-dimensional TDSE. To reduce the reflection from the boundary, a $\cos^{1/8}$ mask function is used at every time step [6]. The convergence of the numerical calculations in this work is achieved by varying the number of basis vectors, and time step. The wave function in Eq. (3) is expanded by 1800 B splines in the radial direction and 48 B splines in the angular ξ direction. The quantum number m is truncated with $|M\max| = 20$. The total number of basis is 3 542 400. 4096 time steps per optical cycle are used in the time propagation. To obtain the initial state, an imaginary time propagation method ($t \to -it$) is used. The angular momentum distributions with orientation angles $\chi = 0^\circ$, 30°, 60°, and 90° are presented in Fig. 2, respectively.

In Fig. 2(a) the laser polarization direction is parallel to the molecular axis along the z axis. One can see that the momentum distributions of photoelectrons with $P_z > 0$ and $P_z < 0$ are quite different. The interference patterns with $P_z > 0$ agree qualitatively with backward scattering holography presented in Figs. 1(c) and 1(d), where we neglect the phase changes due to Coulomb potential. For $P_z < 0$ in Fig. 2(a), the photoelectron momentum distributions correspond to forward scattering holography illustrated in Figs. 1(a) and 1(b). Interestingly one can observe forward and backward scattering interference patterns simultaneously from asymmetric molecules. For $|P_x| < 1$ a.u. and $P_z > 0$, Fig. 2(a) shows an incoming arc structures. The density of patterns becomes small as $|P_z|$ increases, which agrees with Fig. 1(c). For $|P_x| > 1$ a.u. and $P_z > 0$, Fig. 2(a) presents weak interference patterns, similar to Fig. 1(d). We attribute the observation of the backward rescattering holography to the Coulomb focusing effect and small spread of wave packet with short-wavelength laser fields [6]. For $|P_x| < 1$ a.u. and $P_z < 0$, the angular distribution of momentum agrees with Fig. 1(a) and the experiment observations in Ref. [4]. However, the radial interference patterns illustrated in Fig. 1(b), which is difficult to be identified in Ref. [4] due to large spread of wave packets in long-wavelength FEL, can be clearly found in Fig. 2(a). The density of the patterns decreases considerably as $|P_z|$ increases. The width of the stripes becomes large as $|P_z|$ increases, which agrees with the prediction illustrated in Fig. 1(b) by the SFA model. The ultrashort laser pulses used in the present work suppress the ATI rings, which allows clear photoelectron holography to be identified. This demonstrates the second forward rescattering holography and should stimulate experimental efforts to confirm this interference dynamics. The reason why forward and backward rescattering holography can be seen clearly at the same time is that the ionization rates along the $+z$ and $-z$ directions are quite different. The former may be two orders higher than the latter [30] due to resonant excitation to the long-life first excited state $2p\sigma$, which is localized on H^+ [24]. The ionization potential of the right potential well is much lower than the left well. As a result, ionization from the $-z$ direction is negligible. The laser field changes its direction twice per cycle, but only one main photoelectron flux is generated when the laser is along the $+z$ direction. When the laser is along the $-z$ direction, the above photoelectron flux is driven back and rescattered by the molecular cores. So we can unambiguously say that $P_z < 0$ corresponds to forward scattered patterns and $P_z > 0$ are backward scattered patterns. For $|P_x| > 1$ a.u., the scattering angle is near 90°, and the scattering probability is very low. Consequently, the forward and backward rescattered electrons will not overlap, and their corresponding holography patterns can be imaged on the detectors at the same time. The holography pattern is complex compared to the SFA results presented in Fig. 1, where the Coulomb effect is not explicitly included.

When we increase the orientation angle to $\chi = 30^\circ$, the momentum distribution presented in Fig. 2(b) is distorted. The nuclear charges are not parallel to the laser polarization and Coulomb defocusing effects appear. The two Coulomb centers expand the wave packets and reduce the scattering cross sections. The pattern presented in Fig. 1(d) cannot be resolved any more. This channel is the most fragile due to the smallest overlap between the *reference* and *signal* electrons. When the orientation angle $\chi > 60^\circ$, only forward rescattering holography shown in Fig. 1(a) can be seen in Figs. 2(c) and 2(d). The Coulomb defocusing effect dominates with larger orientation angle χ. Consequently, no clear backward rescattering holography can be seen. Even the forward rescattering holography channel in Fig. 1(b) with small overlap disappears.

In summary, We have theoretically studied the orientation dependence of photoelectron holography from the nonsymmetric molecular ion HeH^{2+} in short intense laser pulses. This demonstrates the second kind of forward scattering photoelectron holography illustrated in Fig. 1(b) which is clearly resolved by ultrashort lasers in full quantum simulations. It is also a demonstration that four kinds of photoelectron holography patterns with subcycle interference dynamics can be identified simultaneously with parallel orientation. It is shown that Coulomb focusing effects play a crucial role in the ultrafast scattering processes, which makes the holography patterns rely sensitively on the orientation angles. The present simple HeH^{2+} model system emphasizes that the principle of photoelectron holography is general, and can be used for studying laser-induced electron dynamics in other polar molecules, like HCl [31], CO [32], etc.

We thank RQCHP and Compute Canada for access to massively parallel computer clusters and the CIPI (Canadian Institute for Photonic Innovations) for financial support in its ultrafast science program.

[1] D. Gabor, Nature (London) **161**, 777 (1948).
[2] J. J. Barton, Phys. Rev. Lett. **61**, 1356 (1988).
[3] E. V. van der Zwan and M. Lein, Phys. Rev. Lett. **108**, 043004 (2012).
[4] Y. Huismans *et al.*, Science **331**, 61 (2011).
[5] G. G. Paulus, F. Grasbon, A. Dreischuh, H. Walther, R. Kopold, and W. Becker, Phys. Rev. Lett. **84**, 3791 (2000).
[6] X. B. Bian and A. D. Bandrauk, Phys. Rev. Lett. **108**, 263003 (2012).

[7] X. B. Bian, Y. Huismans, O. Smirnova, K. J. Yuan, M. J. J. Vrakking, and A. D. Bandrauk, Phys. Rev. A **84**, 043420 (2011).
[8] G. G. Paulus, W. Becker, W. Nicklich, and H. Walther, J. Phys. B **27**, L703 (1994).
[9] P. B. Corkum, Phys. Rev. Lett. **71**, 1994 (1993).
[10] A. D. Bandrauk, S. Chelkowski, and S. Goudreau, J. Mod. Opt. **52**, 411 (2005).
[11] T. Marchenko, Y. Huismans, K. J. Schafer, and M. J. J. Vrakking, Phys. Rev. A **84**, 053427 (2011).
[12] T. Brabec, M. Y. Ivanov, and P. B. Corkum, Phys. Rev. A **54**, R2551 (1996).
[13] T. Zuo, A. D. Bandrauk, and P. B. Corkum, Chem. Phys. Lett. **259**, 313 (1996).
[14] M. Peters, T. T. Nguyen-Dang, C. Cornaggia, S. Saugout, E. Charron, A. Keller, and O. Atabek, Phys. Rev. A **83**, 051403 (2011).
[15] G. Dixit, J. M. Slowik, and R. Santra, Phys. Rev. Lett. **110**, 137403 (2013).
[16] R. E. F. Silva, F. Catoire, P. Rivière, H. Bachau, and F. Martín, Phys. Rev. Lett. **110**, 113001 (2013).
[17] G. L. Kamta and A. D. Bandrauk, Phys. Rev. Lett. **94**, 203003 (2005); E. Dehghanian, A. D. Bandrauk, and G. L. Kamta, J. Chem. Phys. **139**, 084315 (2013).
[18] A. Etches and L. B. Madsen, J. Phys. B **43**, 155602 (2010).
[19] H. Akagi *et al*., Science **325**, 1364 (2009).
[20] X. J. Li, S. F. Zhao, and X. X. Zhou, Commun. Theor. Phys. **58**, 419 (2012).
[21] Y. J. Chen, L. B. Fu, and J. Liu, Phys. Rev. Lett. **111**, 073902 (2013).
[22] Y. C. Han, Z. Z. Yu, Y. Huang, and S. L. Cong, J. Chem. Phys. **139**, 044305 (2013).
[23] J. Fernández and L. B. Madsen, Phys. Rev. A **79**, 063406 (2009).
[24] X. B. Bian and A. D. Bandrauk, Phys. Rev. A **86**, 053417 (2012).
[25] I. Ben-Itzhak, I. Gertner, O. Heber, and B. Rosner, Phys. Rev. Lett. **71**, 1347 (1993).
[26] D. D. Hickstein *et al*., Phys. Rev. Lett. **109**, 073004 (2012).
[27] M.-H. Xu, L.-Y. Peng, Z. Zhang, Q. Gong, X.-M. Tong, E. A. Pronin, and A. F. Starace, Phys. Rev. Lett. **107**, 183001 (2011).
[28] W. Quan, Z. Lin, M. Wu, H. Kang, H. Liu, X. Liu, J. Chen, J. Liu, X. T. He, S. G. Chen, H. Xiong, L. Guo, H. Xu, Y. Fu, Y. Cheng, and Z. Z. Xu, Phys. Rev. Lett. **103**, 093001 (2009).
[29] Y. Huismans *et al*., Phys. Rev. Lett. **109**, 013002 (2012).
[30] X. B. Bian and A. D. Bandrauk, Phys. Rev. Lett. **105**, 093903 (2010).
[31] A. Fleischer, H. J. Wörner, L. Arissian, L. R. Liu, M. Meckel, A. Rippert, R. Dörner, D. M. Villeneuve, P. B. Corkum, and A. Staudte, Phys. Rev. Lett. **107**, 113003 (2011).
[32] J. Wu, L. Ph. H. Schmidt, M. Kunitski, M. Meckel, S. Voss, H. Sann, H. Kim, T. Jahnke, A. Czasch, and R. Dörner, Phys. Rev. Lett. **108**, 183001 (2012).